

Haruo Watanabe
Masayuki Kanematsu
Teruhiko Kitagawa
Yuriko Suzuki
Hiroshi Kondo
Satoshi Goshima
Kimihiro Kajita
Kyongtae T. Bae
Yoshinobu Hirose
Seiki Miotani
Xiangrong Zhou
Hiroshi Fujita

MR elastography of the liver at 3 T with cine-tagging and bending energy analysis: preliminary results

Received: 31 October 2009
Revised: 23 February 2010
Accepted: 24 February 2010
Published online: 4 May 2010
© European Society of Radiology 2010

H. Watanabe (✉) · M. Kanematsu ·
H. Kondo · S. Goshima · K. Kajita
Department of Radiology,
Gifu University Hospital,
1-1 Yanagido, 501-1194 Gifu, Japan
e-mail: haruwow860@yahoo.co.jp

T. Kitagawa
Department of Electronic Control
Engineering,
Gifu National College of Technology,
Motosu, Japan

Y. Suzuki
Philips Electronics Japan Ltd., Medical
Systems, Tokyo, Japan

K. T. Bae
Department of Radiology,
University of Pittsburgh Medical Center,
Pittsburgh, PA, USA

Y. Hirose
Department of Pathology,
Gifu University Hospital, Gifu, Japan

S. Miotani · X. Zhou · H. Fujita
Department of Intelligent Image
Information, Division of Regeneration
and Advanced Medical Sciences,
Graduate School of Medicine,

Abstract

Objective: To preliminarily evaluate the feasibility and usefulness of MR elastography of the liver at 3 T with cine-tagging and bending energy (BE) analysis for the evaluation of hepatic fibrosis. **Materials and Methods:** Twenty-two patients underwent MR elastography with four different cine-tagging grids on the liver (16- or 20-mm sagittal or coronal). Nine images serially obtained during 1-s of exhalation were analyzed to define coordinates of grid intersections. BE

values were calculated using the thin-plate spline method. BE values were compared among patient groups with different fibrosis stage thresholds.

Results: In the 22 patients, six had a fibrosis score of F0, one had F1, seven had F2, three had F3, and five had F4. Mean BE value with 16-mm sagittal grid was greater with fibrosis score F0 (1.54 ± 0.63) than with $\geq F1$ (0.97 ± 0.12 , $P=0.013$) as well as with $\leq F1$ (1.48 ± 0.60) than with $\geq F2$ (0.96 ± 0.36 , $P=0.019$). **Conclusion:** Our results showed that MR elastography with 16-mm sagittal grid and BE analysis had a potential in discrimination for the patients with moderate or advanced hepatic fibrosis from those with healthy liver or slight fibrosis.

Keywords MR imaging · Liver fibrosis · 3 Tesla · Elastography · Cine-tagging

Introduction

Patients with chronic hepatitis or cirrhosis have a great risk of complications such as hepatocellular carcinoma and liver failure [1]. The degree of hepatic fibrosis is a critical predictive factor for the occurrence of hepatocellular carcinoma [2], and the cumulative incidence of hepatocellular carcinoma was significantly higher in patients with severe fibrosis than in those with no or mild fibrosis [3]. Furthermore, the stage of hepatic fibrosis is considered to determine the treatment options as well as to estimate the prognosis.

To date, there have been several methods for assessing the degree of hepatic fibrosis. Although liver biopsy is the current standard of reference for determining fibrosis

stage, it is invasive and the accuracy may be questioned because of sampling and interobserver variability in the determination of semiquantitative fibrosis scores [4, 5]. Therefore, research has been focused on the evaluation of noninvasive methods, including kinds of hematological or radiological examinations. Some hematological markers, such as aspartate aminotransferase-to-platelet ratio index (APRI) [6, 7] or fibroindex [8], have been used in clinical practice, and it has been reported that these markers have a sufficient correlation with the degree of hepatic fibrosis. Recently, however, radiological assessments of hepatic fibrosis by magnetic resonance (MR) elastography [9–11], gadolinium- or superparamagnetic iron oxide (SPIO)-enhanced MR imaging [12, 13], diffusion-weighted MR

imaging [14], real-time ultrasonographic elastography [15], and computer-aided diagnosis of MR images [16] have been reported, and their feasibility, usefulness, and limitations have been shown.

Meanwhile, cine-tagging MR imaging of the heart using a spatial modulation of magnetization (SPAMM) sequence [17, 18] is a useful tool to evaluate the kinetics of cardiac muscles. Cine-tagging MR imaging can provide supplementary information about wall motion, which enables the detection of hypokinetic myocardial segments [19–22]. Although a limitation of MR cine-tagging at 1.5 T was that the tag lines fade and the edges blur shortly due to longitudinal relaxation [17–20], the tag lines at 3 T may well last longer due to prolonged T1 relaxation times of organs [23].

We postulated that prospective improvement in quality of MR cine-tagging owing to elongated T1 relaxation time of the liver at higher magnetic field (586 ms at 1.5 T and 809 ms at 3 T) [23] would enable more accurate evaluation of liver stiffness by means of bending energy (BE) analysis using the thin-plate spline method [24]. Hence, the purpose of our study was to preliminarily evaluate the feasibility and the potential usefulness of MR elastography of the liver at 3 T with cine-tagging and BE analysis for the evaluation of hepatic fibrosis.

Materials and methods

Cine-tagging MR image acquisition

All MR imaging was performed with a 3-T superconducting system (Intera Achieva Quasar Dual; Philips Medical Systems, Netherlands) with a six-channel torso array coil. We employed a modified SPAMM sequence with a train of nonselective radiofrequency (RF) pulses, the relative amplitudes of which were distributed according to the binomial coefficients of 1-3-3-1 (Fig. 1) [17–19]. The absolute amplitudes were adjusted for the total amplitude of the modulation desired. Separating each of the RF pulses was a gradient pulse oriented perpendicularly to the desired stripe



Fig. 1 Diagram showing the pulse sequence architecture of the binomial SPAMM sequence for two-dimensional grid formation prior to cine imaging. G_x , G_y , and G_z are gradients in the x -, y - and z -axes, respectively. Radiofrequency (RF) pulse amplitudes are distributed as 1-3-3-1 for sharper-edged grid. Gradients G_x and G_y are orthogonal to produce orthogonal sets of stripes. Gradient pulses used for modulation have amplitude and duration such that the area under the pulse shape is inversely proportional to the desired stripe spacing. Spoiler gradients are used after binomial SPAMM pulses to dephase remaining transverse magnetization

orientation and with a strength and duration dependent on the desired stripe spacing. For the gradient amplitude G , the stripe spacing was equal to the reciprocal of $\gamma|G\delta t$, where γ was the gyromagnetic ratio. A grid formed with stripes perpendicular to each other was produced by following the initial SPAMM sequence with a second one, with the gradient oriented perpendicularly to the initial one. A gradient spoiler was applied after the SPAMM sequence to dephase remaining transverse magnetization. The tagging grids faded at a rate determined by the local T1 relaxation times (liver; 809 ms at 3 T) [23].

Sequentially after the SPAMM sequence, single-section cine MR imaging with a two-dimensional single-shot turbo field-echo sequence (TR/TE, 2.2/1.0 ms; flip angle, 10° ; field of view, 45×36 cm; number of echo train, 35; interpolated imaging matrix, 256×256 ; parallel imaging factor, 2; slice thickness; 10 mm, nine images during 1 s) was conducted (Fig. 2). The SPAMM sequence and cine imaging were serially run during a forced exhalation by patients. Patients were instructed in advance to exhale at a constant speed over 1 s from maximal inspiratory to maximal expiratory phases, and they practiced a few times until the attending MR technicians confirmed that the exhalation was done virtually at a constant speed, monitoring the respiratory phase curve displayed with a commercially available pressure monitoring device routinely put on the patient abdomen.

For determining optimal stripe spacing and imaging plane of cine-tagging grids, we had performed a preliminary unpublished study and selected 12-, 16-, 20- and 24-mm spacing. We assessed that a 12-mm spacing was too small to clearly identify crossing points in the BE analysis and 24 mm was too large to have a sufficient number of coordinate samples, especially in small cirrhotic livers. Thus, we chose 16- and 20-mm stripe spacing and sagittal and coronal planes, resulting in four different cine-tagging methods: the liver was imaged four times separately using a 16-mm sagittal, 20-mm sagittal, 16-mm coronal, and a 20-mm coronal grid (Fig. 3). We set sagittal grids in the right hepatic lobe, so the sagittal plane did not include the heart or porta hepatis and the cross-sectional area of liver was as large as possible; typically the sagittal plane was set at the top of the right hemidiaphragm. On the other hand, we set the coronal grids in the liver, so the coronal plane included the right and left hepatic lobes as broad as possible, typically at a ventral one-third of the entire anteroposterior dimension of the liver. The changing configuration of the grid pattern during 1-s of forced exhalation reflected the local motion, rotation, deformation, or distortion of the liver parenchyma.

Data procession and BE analysis

A radiologist (H.W.) with 3-years' experience in MR imaging diagnosis of the abdomen subjectively determined the coordinate values of intersecting points of grids on the first (before warping) and the last (after warping) images, observing continuous deformation of the grids in nine cine images on a commercially available DICOM viewer. The

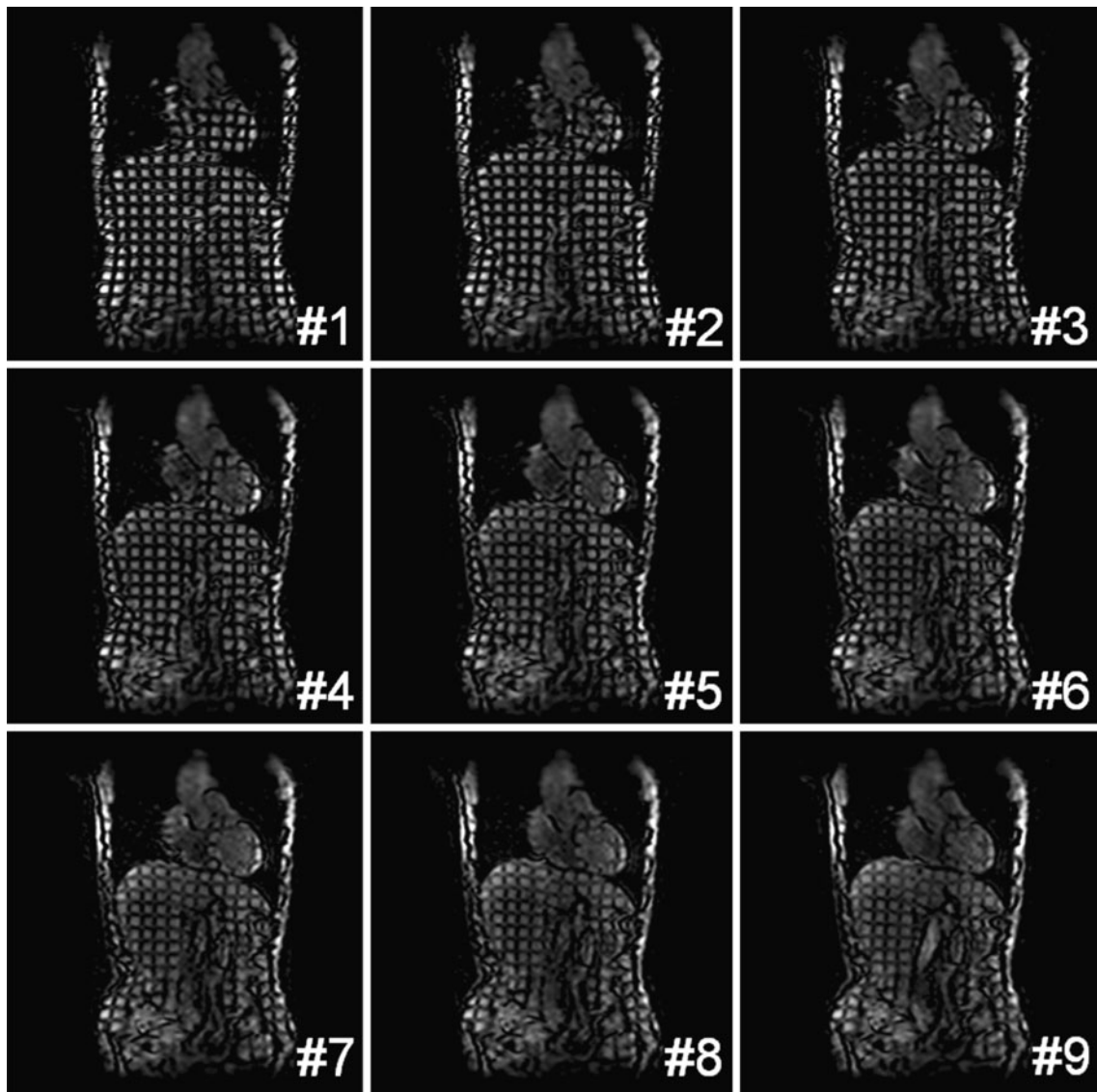


Fig. 2 Coronal MR images showing a series of nine cine-tagging images obtained during 1-s of forced exhalation using the 16-mm coronal grid in a 75-year-old male patient with healthy liver (F0). The numbers shown at the right bottom of images indicate the order of cine images obtained serially. The cine images were obtained from the maximal inspiratory phase (1) to the maximal expiratory

phase (9). Coordinate values of the grid intersections were measured on the first (1 before warping) and the last (9 after warping) images, referring to the intermediate images (2–8). Note that the grid fades in signal intensity from image 1 to image 9, but that image quality is sufficient to define the coordinates with a cursor. Also note that the grid is deformed during forced exhalation

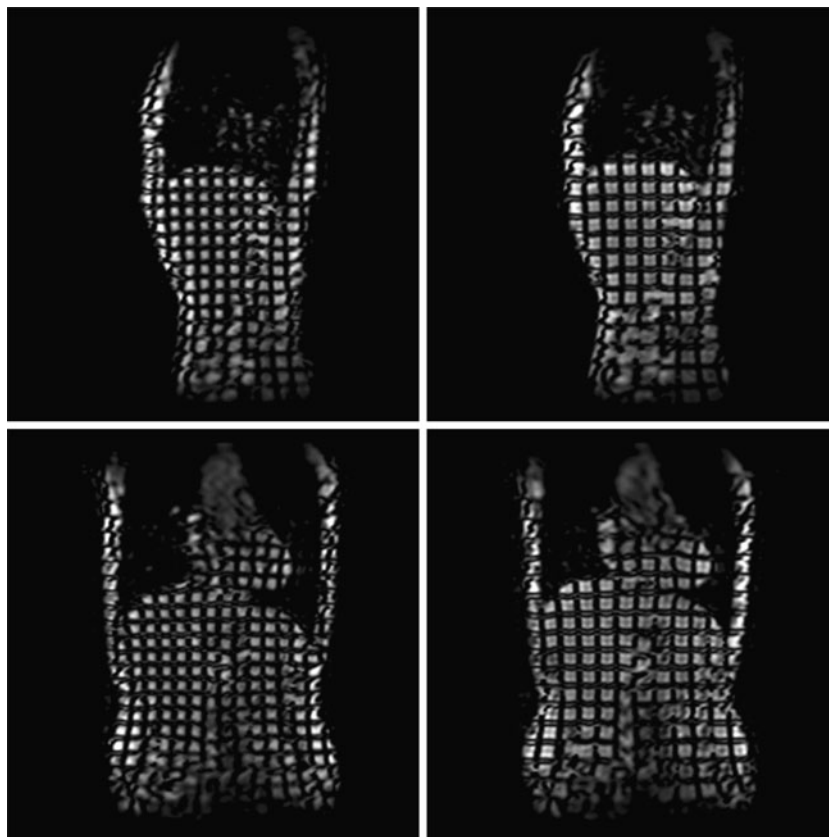
viewer displayed coordinate values in integers (x, y) of the center of a crosshair cursor manually placed on images, and the coordinates could range from (0, 0) to (256, 256) in 256×256 matrix images. As the grid lines were 5-mm thick for both 16- and 20-mm grids, the radiologist placed the center of the crosshair cursor carefully on the very center of grid intersections to measure coordinates. The radiologist sampled the coordinate values on the grid devoid of those right on the margins of the liver, but included those near the margins, in the left liver lobe, and under the heart and hemidiaphragms, when the crossing points on the grid were visually confirmed. Thus, the first coordinates (x, y) and the last coordinates (x_i, y_i) of the grid intersections in the four different kinds of cine-tagging images were recorded for each patient.

The coordinate values were processed to quantify the degree of distortion or deformation of liver parenchyma. We applied a “thin plate spline” referring to a physical analogy involving the bending of a thin sheet of metal which has been well recognized and used extensively in engineering [24] to calculate BE values (Appendix).

Reproducibility assessment with healthy volunteers

Ten healthy male volunteers, ranged in age from 23 to 29 years (mean, 26 years), with no history of liver disease, underwent cine-tagging MR imaging of the liver and informed consent was obtained from them. Cine-tagging MR imaging with the four different grids was performed

Fig. 3 The first cine-tagging images obtained in a 75-year-old male patient with a healthy liver at the maximal inspiratory phase, using 16-mm sagittal (*top left*), 20-mm sagittal (*top right*), 16-mm coronal (*bottom left*), and 20-mm coronal (*bottom right*) grids. Note that the number of grid intersections is greater with smaller strip spacing



in each healthy volunteer. Cine-tagging MR imaging with the same grid was repeated three times each for the assessment of reproducibility of the MR elastography.

Patients

This study was approved by our institutional review board and informed consent was obtained from all patients. Cine-tagging MR imaging was added to our routine MR imaging protocol of the liver consisted of the following sequences: dual-echo T1-weighted fast field-echo [repetition time (TR)/echo time (TE), 292/2.3 ms at in-phase and 292/1.1 ms at opposed-phase; number of signals averaged, 1; slice thickness, 6 mm with a 1-mm gap; breath-hold acquisition time for 30 slices each at in-phase and opposed-phase, 25 s]; fat-suppressed respiration-triggered T2-weighted turbo spin-echo (effective TR /effective TE, 1,200-3,600/80 ms; number of signals averaged, 2; slice thickness, 6 mm with a 1-mm gap; acquisition time for 30 slices, 1.5 min); and breath-hold gadolinium-enhanced early hepatic arterial, late hepatic arterial, portal venous, and equilibrium phase imaging with fat-suppressed three-dimensional spoiled fast field-echo (TR/TE, 4.0/2.1 ms, flip angle, 12°; slice thickness, 4-mm section thickness with a 2-mm overlap; acquisition time for 90 slices during each phase, 12 s). Cine-tagging MR imaging was performed before gadolinium-enhanced imaging to avoid undesired T1 shortening of the liver parenchyma.

Eighty-one consecutive patients suspected of having hepatic disease by previously performed ultrasonography, CT, or laboratory test results underwent liver MR imaging including cine-tagging MR elastography at our hospital during a 3-month period. After study inclusion, 54 patients who had previously undergone partial hepatectomy for malignant hepatic tumors were excluded from the current investigation because of concerns that a preceding surgery might have caused adhesion or focal fibrosis inside or outside the liver, and these conditions might adversely affect the evaluation and five were removed because their liver biopsy findings were unsuitable for fibrosis staging.

The remaining 22 patients formed our study cohort [13 men and nine women, age range 50–82 years (mean, 68.0 years)]. In the 22 patients, percutaneous liver biopsy ($n=13$) and partial hepatectomy ($n=9$) was performed after MR imaging. The biopsy was performed for patients with hepatic tumors ($n=7$) and those before interferon therapy ($n=6$). In tumor biopsy the surrounding liver parenchymal tissue was sampled as well. Partial hepatectomy was performed for malignant hepatic tumors (hepatocellular carcinoma, $n=6$; metastasis, $n=3$).

The cause of chronic liver disease was viral in 15 patients (type C in 13 and type B in two) and cryptogenic in two. All biopsy and surgical specimens were evaluated by a board hepatopathologist with 15-years' experience, who was blinded to the results of MR elastography. The fibrosis stage was evaluated semiquantitatively according

Table 1 Number of coordinates measured on cine-tagging images. (The data are in ranges, with the mean \pm 1 SD in parentheses)

| Hepatic fibrosis grade | Number of coordinates | | | |
|------------------------|-------------------------|-------------------------|-------------------------|-------------------------|
| | 16-mm sagittal grid | 20-mm sagittal grid | 16-mm coronal grid | 20-mm-coronal grid |
| F0 (<i>n</i> =6) | 44–74 (59.0 \pm 13.6) | 36–50 (45.3 \pm 5.5) | 56–94 (70.0 \pm 14.6) | 30–68 (50.7 \pm 12.9) |
| F1 (<i>n</i> =1) | 64 | 48 | 66 | 36 |
| F2 (<i>n</i> =7) | 38–86 (49.5 \pm 18.3) | 26–58 (40.3 \pm 12.5) | 36–66 (51.3 \pm 12.8) | 32–54 (40.0 \pm 7.9) |
| F3 (<i>n</i> =3) | 58–82 (66.7 \pm 13.3) | 36–50 (44.0 \pm 7.2) | 50–84 (70.7 \pm 18.5) | 44–56 (48.0 \pm 6.9) |
| F4 (<i>n</i> =5) | 42–82 (62.4 \pm 16.5) | 34–48 (41.6 \pm 5.0) | 38–68 (52.0 \pm 13.3) | 24–54 (43.2 \pm 13.1) |
| All (<i>n</i> =22) | 38–86 (58.4 \pm 15.6) | 26–58 (42.8 \pm 8.2) | 36–94 (60.3 \pm 15.8) | 24–68 (44.6 \pm 10.8) |

to the following: F0 means no fibrosis; F1, portal fibrosis without septa; F2, portal fibrosis and a few septa; F3, numerous septa without cirrhosis; F4, cirrhosis.

Statistical analyses

To evaluate the reproducibility of the technique, the intraclass correlation coefficients were calculated for BE values in the ten healthy volunteers. BE values in the 22 patients were compared among the fibrosis stages using the unpaired *t*-test. The diagnostic performances of BE values calculated by four different grids for the detection of hepatic fibrosis were determined as areas under curve (AUCs) by using receiver-operating characteristic (ROC) curve analysis (ROCKIT 0.9B, Charles E. Metz, The University of Chicago), and the AUCs were compared between the four different grids. We considered a *P* value less than 0.05 significant for the intraclass correlation coefficients and unpaired *t*-tests. We used a stricter *P* value of less than 0.0083 for comparison of AUCs, introducing the Bonferroni correction.

Results

MR cine-tagging was successfully performed in all healthy volunteers and patients without any adverse events or technical failures during image acquisitions. The image quality was sufficient to define and measure coordinates on cine-tagging grids in all patients. In healthy volunteers, the intraclass correlation coefficients were 0.75 (*P*=0.004), 0.59 (*P*=0.046), 0.83 (*P*<0.001), and 0.83 (*P*=0.001) with the BE values calculated using the 16-mm sagittal, 20-mm sagittal, 16-mm coronal, and 20-mm

coronal grids, respectively. Sufficiently high reproducibility of the method was confirmed.

Six (27%) of the 22 patients had a fibrosis score of F0, one (4%) had F1, seven (32%) had F2, three (14%) had F3 and five (23%) had F4. The BE values were successfully calculated with all four kinds of grids in all patients, and the value ranged from 0.07 to 2.58 (mean \pm 1 SD, 0.84 \pm 0.48), and the number of coordinates sampled on a grid ranged from 24 to 94 (mean \pm 1 SD, 51.3 \pm 15.0), depending on a combination of size of the liver, stripe spacing, and imaging plane (Tables 1, 2). The mean BE value calculated using a 16-mm sagittal grid was significantly greater, with the fibrosis score 0 (F0) (1.54 \pm 0.63), than with \geq F1 (0.97 \pm 0.12, *P*=0.013) as well as with \leq F1 (1.48 \pm 0.60) than with \geq F2 (0.96 \pm 0.36, *P*=0.019) (Table 3, Figs. 4, 5, 6).

The mean BE value calculated with the 20-mm sagittal grid was marginally greater with F0 (1.19 \pm 0.45) than with \geq F1 (0.78 \pm 0.47) as well as with \leq F1 (1.18 \pm 0.41, *P*=0.078) than with \geq F2 (0.76 \pm 0.48, *P*=0.057).

In the detection of hepatic fibrosis \geq F1 and \geq F2, the area under ROC curves (AUCs) determined by BE values was larger with the 16-mm sagittal grid than with the other grids, although no significant difference was found (Table 4).

Discussion

We here preliminarily report a new methodology of MR elastography for the liver with cine-tagging MR imaging at 3 T and BE analysis for the evaluation of hepatic fibrosis. The BE values are generally invariant to evaluate the degree of distortion or deformation of a non-rigid object and would make it possible to evaluate the quantitative stiffness of the liver. Comparing the four

Table 2 Bending energy values calculated with cine-tagging images. (The data are in ranges, with the mean \pm 1 SD in parentheses)

| Hepatic fibrosis grade | Bending energy value | | | |
|------------------------|-----------------------------|-----------------------------|-----------------------------|-----------------------------|
| | 16-mm sagittal grid | 20-mm sagittal grid | 16-mm coronal grid | 20-mm coronal grid |
| F0 (<i>n</i> =6) | 1.03–2.58 (1.54 \pm 0.63) | 0.81–1.88 (1.19 \pm 0.45) | 0.27–1.27 (0.83 \pm 0.39) | 0.29–1.04 (0.62 \pm 0.26) |
| F1 (<i>n</i> =1) | 1.13 | 1.11 | 0.16 | 0.67 |
| F2 (<i>n</i> =7) | 0.58–1.13 (0.81 \pm 0.22) | 0.34–0.89 (0.54 \pm 0.23) | 0.25–0.93 (0.65 \pm 0.25) | 0.14–1.23 (0.70 \pm 0.39) |
| F3 (<i>n</i> =3) | 1.09–1.91 (1.37 \pm 0.46) | 0.41–2.12 (1.09 \pm 0.91) | 0.29–1.42 (0.82 \pm 0.57) | 0.53–2.19 (1.18 \pm 0.89) |
| F4 (<i>n</i> =5) | 0.54–1.39 (0.94 \pm 0.32) | 0.25–1.19 (0.86 \pm 0.36) | 0.31–0.59 (0.50 \pm 0.11) | 0.07–0.46 (0.32 \pm 0.16) |
| All (<i>n</i> =22) | 0.54–2.58 (1.13 \pm 0.50) | 0.25–2.12 (0.89 \pm 0.49) | 0.16–1.42 (0.66 \pm 0.34) | 0.07–2.19 (0.66 \pm 0.45) |

Table 3 Bending energy values calculated with the four grids for each fibrosis score threshold. (The data are in ranges, with the mean \pm 1 SD in parentheses)

| Hepatic fibrosis grade | Bending energy value | | | |
|------------------------|------------------------------|------------------------------|--------------------|--------------------|
| | 16-mm sagittal grid | 20-mm sagittal grid | 16-mm coronal grid | 20-mm coronal grid |
| F=0 (n=6) | 1.54 \pm 0.63 ^a | 1.19 \pm 0.45 ^c | 0.83 \pm 0.39 | 0.62 \pm 0.26 |
| F \geq 1 (n=16) | 0.97 \pm 0.12 | 0.78 \pm 0.47 | 0.60 \pm 0.31 | 0.69 \pm 0.52 |
| F \leq 1 (n=7) | 1.48 \pm 0.60 ^b | 1.18 \pm 0.41 ^d | 0.73 \pm 0.43 | 0.63 \pm 0.24 |
| F \geq 2 (n=15) | 0.96 \pm 0.36 | 0.76 \pm 0.48 | 0.63 \pm 0.30 | 0.67 \pm 0.53 |
| F \leq 2 (n=14) | 1.14 \pm 0.56 | 0.86 \pm 0.46 | 0.69 \pm 0.34 | 0.67 \pm 0.31 |
| F \geq 3 (n=8) | 1.10 \pm 0.41 | 0.94 \pm 0.57 | 0.62 \pm 0.36 | 0.64 \pm 0.66 |
| F \leq 3 (n=17) | 1.18 \pm 0.53 | 0.90 \pm 0.53 | 0.71 \pm 0.37 | 0.76 \pm 0.47 |
| F=4 (n=5) | 0.94 \pm 0.32 | 0.86 \pm 0.36 | 0.50 \pm 0.11 | 0.32 \pm 0.16 |

^a The value was significantly greater than that with F \geq 1 ($P=0.013$).

^b The value was significantly greater than that with F \geq 2 ($P=0.019$).

^c The value was marginally greater than that with F \geq 1 ($P=0.078$).

^d The value was marginally greater than that with F \geq 2 ($P=0.057$).

different types of grids, the mean BE values output by the 16-mm sagittal grid were significantly greater for patients with hepatic fibrosis F0 than for those \geq F1 as well as for \leq F1 than for \geq F2, respectively. The reason why the 16-mm sagittal grid showed the best performance in the diagnosis was deduced as follows: the smaller the strip spacing, the greater the number of sampled coordinates, which resulted in a more accurate calculation of BE values using the thin-plate spline method.

With regards to the choice of imaging plane, sagittal grids more accurately reflected the degree of chronic liver damage than coronal grids. The stiffness of the liver parenchyma would be underestimated using coronal grids because deformity of the entire liver across the right and left hepatic lobes might be overemphasized by the compression of the heart when using coronal grids. Accordingly, such influence was less marked with the

sagittal grids placed in the right hepatic lobe and the liver stiffness was more purely reflected by sagittal grids. In the coronal grids, when both hemidiaphragms moved upward during exhalation, right and left hepatic lobes were simultaneously retracted upwards. However, the central portion of the liver, typically the proximal portion of the left lateral lobe, did not move very much, because of the heart abutting the liver superiorly. In any event, a large amount of deformity of the entire liver took place in the coronal grids, regardless of the presence of hepatic fibrosis. Even though livers with hepatic fibrosis were stiffer than normal livers, they were compelled to be

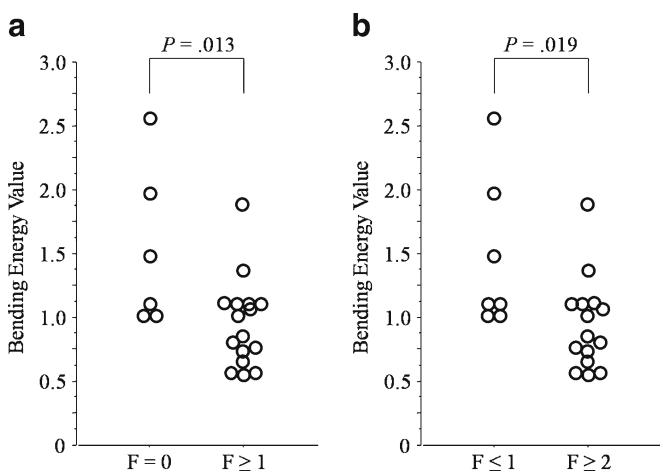


Fig. 4 Scatter diagrams of the BE values calculated with the 16-mm sagittal grid for fibrosis score threshold. **a** The BE values with the 16-mm sagittal grid were significantly greater ($P=0.013$) in patients with no hepatic fibrosis, F0 (1.54 \pm 0.63) than in those with hepatic fibrosis \geq F1 (0.97 \pm 0.12). **b** The BE values with the 16-mm sagittal grid were significantly greater ($P=0.019$) in patients with hepatic fibrosis \leq F1 (1.48 \pm 0.60) than in those \geq F2 (0.96 \pm 0.36)

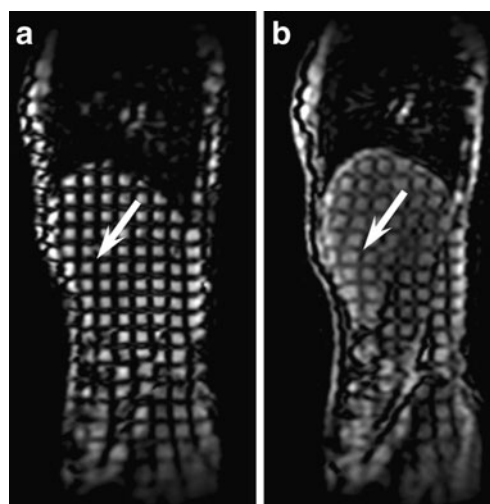


Fig. 5 Cine-tagging images using a 16-mm sagittal grid in a 56-year-old male patient with fibrosis scores equal to F0. The first image (**a**) obtained at the maximum inspiratory phase shows the grid without distortion. The last image (**b**) obtained at the maximum expiratory phase shows the grid with evident distortion. For example, coordinate values of a given grid intersection on the first image (x, y) (arrow in **a**) and those of the corresponding grid intersection on the last image (x_i, y_i) (arrow in **b**) were sampled by a radiologist observing continuous deformation of the grids through the nine cine images. Likewise, all the other coordinate values in the liver were sampled. The BE value calculated using these images was 2.52

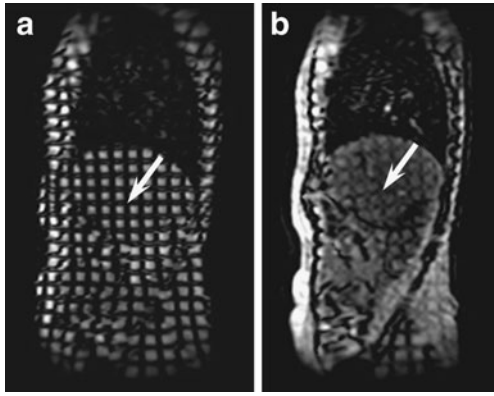


Fig. 6 Cine-tagging images using a 16-mm sagittal grid in a 72-year-old male patient with fibrosis scores equal to F4. The first image (a) obtained at the maximum inspiratory phase shows the grid without distortion. The last image (b) obtained at the maximum expiratory phase shows the grid rotated slightly counterclockwise, but there is no distortion with the grid. For example, coordinate values of a given grid intersection on the first image (x, y) (arrow in a) and those of the corresponding grid intersection on the last image (x_i, y_i) (arrow in b) were sampled by a radiologist observing continuous rotation of the grids through the nine cine images. Likewise, all the other coordinate values in the liver were sampled. The BE value calculated using these images was as low as 0.57

deformed in the coronal plane during exhalation, because of the simultaneous large superior pull by the lungs and relative inferior push from the heart affecting the liver.

Interestingly, BE values were generally larger for the sagittal grids than for the coronal grids. We postulated the reason as follows: the posterobasal segments of lung most actively deflated and shrank during forced exhalation, and such large motions were more directly reflected to the BE values in the sagittal grids that included the dorsal segments of the liver. However, the coronal grids were typically placed in the ventral portion of the liver and did not include the dorsal portion of the liver, resulting in smaller BE values due to less influenced movement of the posterobasal segments of the lung. For all these reasons, we infer that the use of sagittal grids with smaller stripe spacing would be optimal for the purpose of cine-tagging MR imaging of the liver.

Recently, several radiological methods have been reported, and some of these techniques were highly correlated with the degree of hepatic fibrosis [8–16]. Researchers at the Mayo Clinic first reported the methodology of MR elastography by direct visualization of propagating acoustic strain waves [9], and afterward they reported preliminary results showing the usefulness of MR elastography [10], although there were some overlaps of

shear stiffness in kilopascal among the intermediate fibrosis stages. Huwart et al. [11] also described the usefulness of MR elastography using a similar method and concluded that MR elastography was accurate in hepatic fibrosis staging and superior to biochemical testing with APRI, based on their results of large AUCs for elasticity (>0.99 for scores $\geq F2$, $\geq F3$, and F4).

In our preliminary results, our new method enabled separation of patients with healthy liver or slight hepatic fibrosis and moderate or advanced hepatic fibrosis to a certain extent, although there still were some overlaps. Compared with previous methods, our method had several advantages for the following reasons. First, ours required no contrast media [12, 13] or particular mechanical devices [9–11]. Second, if limited to the use of 16-mm sagittal grid, cine-tagging imaging would be typically completed within 2 min, including localization, preparation scan, practice of breathing, and imaging, so it could be incorporated into a routine liver imaging protocol except that it took approximately 10 min for the manual post-processing to define the coordinates and calculate BE values. As there was no need to conduct shear waves or ultrasound to the liver through the body walls in our method, influences of ascites, thick subcutaneous fat in obese patients, or thick muscles in large patients would be less than in previously reported MR or ultrasonographic elastography [9–11, 15]. Our method would propose visually perceivable dynamic motion and distortion of the liver parenchyma during respiration and might help radiologists visually evaluate stiffness of the liver. Our preliminary results indicated that this technique potentially has the capability to facilitate noninvasive assessment of hepatic fibrosis. Moreover, a BE mapping may well be a target for further evaluation using our method, because hepatic fibrosis is often unevenly distributed in the liver and histopathological diagnosis by percutaneous biopsy has limitations. If a BE mapping of the liver is realized, our method might be an early indicator for local disturbances in terms of progress of fibrosis to cirrhosis in diffuse liver disease.

There were some limitations to our study associated with the study design and the technical aspects. First, the size of the cohort was not large enough. Evaluation of diagnostic performance in a large cohort correlated with fibrosis stages is necessary to determine if this method is able to play a decisive role in the management of patients with suspected hepatic fibrosis. Second, although careful attention was paid to maintain unification with cine-scan timing during forced exhalation patients to patients, there might have been some intra- or inter-subjective variability

Table 4 AUC values with the four grids according to fibrosis score

| Hepatic fibrosis grade | AUC values | | | |
|------------------------|---------------------|---------------------|--------------------|--------------------|
| | 16 mm-sagittal grid | 20 mm-sagittal grid | 16 mm-coronal grid | 20 mm-coronal grid |
| F \geq 1 ($n=16$) | 0.798 | 0.768 | 0.713 | 0.503 |
| F \geq 2 ($n=15$) | 0.802 | 0.791 | 0.594 | 0.540 |
| F \geq 3 ($n=8$) | 0.471 | 0.475 | 0.529 | 0.584 |
| F=4 ($n=5$) | 0.629 | 0.459 | 0.712 | 0.871 |

as well as intra- and inter-operator variability. Taking an average of BE values obtained during multiple sessions may reduce intra- and inter-subjective variability. Consequently, we now apply a navigator echo technique to the right hepatic lobe so the operators can monitor the motion of the liver accurately and unify the cine-scan timing. Third, this study was conducted as preliminary technical development research, and considerable time and effort were expended to manually define the coordinates and recorded the values. We have now started to develop an automated algorithm to calculate BE values with cine-tagging MR images. Fourth, theoretically, there was no reason why BE values for F2 were smaller than those for F3 and F4 other than due to methodological errors or shortage in number of cohort. There was no statistical difference between the BE values with F2 and F3/F4, so we believe that the values would have been very closer, had we recruited more cases into the study. Another possible cause was that we determined F grades by biopsy specimen in some cases, and an accurate correlation between BE value and degree of fibrosis might have been spoiled in those cases. Finally, our method did not allow measurements of stiffness of the liver shown by absolute values such as numeric values in kilopascals.

In conclusion, our preliminary study showed that cine-tagging MR imaging with the 16-mm sagittal grid and the BE analysis enabled discrimination of patients with moderate or advanced hepatic fibrosis from those with

healthy liver or slight hepatic fibrosis to a certain extent. This method, which required no contrast agents or mechanical devices and enabled direct visualization of hepatic motion and distortion, was considered to have a potential as an alternative tool for the evaluation of hepatic fibrosis. This MR elastography might be more practically incorporated into an MR imaging protocol if the output of BE values was automated.

Acknowledgements This work was supported by Japan Society for the Promotion of Science KAKENHI (20591439) and in part by the Health and Labour Sciences Research Grants for Third Term Comprehensive Control Research for Cancer.

Appendix

The BE is invariant for movements of the liver such as rotation and translation and is only related to the energy that is used to deform the liver parenchyma. This property makes it very suitable to provide a quantitative measure of softness of the liver in cine-tagging MR images. The number of the points that were used to show the liver is an important parameter during the BE computations. This theory is used in non-rigid warping method known as thin plate spline [24].

References

1. El-Serag HB, Mason AC (1999) Rising incidence of hepatocellular carcinoma in the United States. *N Engl J Med* 340:745–750
2. Yatsuhashi H, Yano M (2000) Natural history of chronic hepatitis C. *J Gastroenterol Hepatol* 15:111–116
3. Tokita H, Fukui H, Tanaka A et al (2005) Risk factors for the development of hepatocellular carcinoma among patients with chronic hepatitis C who achieved a sustained virological response to interferon therapy. *J Gastroenterol Hepatol* 20:752–758
4. Bravo AA, Sheth SG, Chopra S (2001) Liver biopsy. *N Engl J Med* 344:495–500
5. Regev A, Berho M, Jeffers LJ et al (2002) Sampling error and intraobserver variation in liver biopsy in patients with chronic HCV infection. *Am J Gastroenterol* 97:2614–2618
6. Snyder N, Gajula L, Xiao SY et al (2006) APRI: an easy and validated predictor of hepatic fibrosis in chronic hepatitis C. *J Clin Gastroenterol* 40:535–542
7. Wai CT, Greenon JK, Fontana RJ et al (2003) A simple noninvasive index can predict both significant fibrosis and cirrhosis in patients with chronic hepatitis C. *Hepatology* 38:518–526
8. Koda M, Matunaga Y, Kawakami M et al (2007) FibroIndex, a practical index for predicting significant fibrosis in patients with chronic hepatitis C. *Hepatology* 46:280–281
9. Muthupillai R, Lomas DJ, Rossman PJ et al (1995) Magnetic resonance elastography by direct visualization of propagating acoustic strain waves. *Science* 269:1854–1857
10. Rouvière O, Yin M, Dresner MA et al (2006) MR elastography of the liver: preliminary results. *Radiology* 240:440–448
11. Huwart L, Sempoux C, Salameh N et al (2007) Liver fibrosis: noninvasive assessment with MR elastography versus aspartate aminotransferase-to-platelet ratio index. *Radiology* 245:458–466
12. Lucidarme O, Baleston F, Cadi M et al (2003) Non-invasive detection of liver fibrosis: is superparamagnetic iron oxide particle-enhanced MR imaging a contributive technique? *Eur Radiol* 13:467–474
13. Aguirre DA, Behling CA, Alpert E et al (2006) Liver fibrosis: noninvasive diagnosis with double contrast material-enhanced MR imaging. *Radiology* 239:425–437
14. Taouli B, Tolia AJ, Losada M et al (2007) Diffusion-weighted MRI for quantification of liver fibrosis: preliminary experience. *AJR Am J Roentgenol* 189:799–806
15. Friedrich-Rust M, Ong MF, Herrmann E et al (2007) Real-time elastography for noninvasive assessment of liver fibrosis in chronic viral hepatitis. *AJR Am J Roentgenol* 188:758–764

-
16. Kato H, Kanematsu M, Zhang X et al (2007) Computer-aided diagnosis of hepatic fibrosis: preliminary evaluation of MRI texture analysis using the finite difference method and an artificial neural network. *AJR Am J Roentgenol* 189:117–122
 17. Zerhouni EA, Parish DM, Rogers WJ et al (1988) Human heart: tagging with MR imaging—a method for noninvasive assessment of myocardial motion. *Radiology* 169:59–63
 18. Axel L, Dougherty L (1989) MR imaging of motion with spatial modulation of magnetization. *Radiology* 17:841–845
 19. Axel L, Dougherty L (1989) Heart wall motion: improved method of spatial modulation of magnetization for MR imaging. *Radiology* 172:349–350
 20. Bolster BD Jr, McVeigh ER, Zerhouni EA (1990) Myocardial tagging in polar coordinates with use of striped tags. *Radiology* 177:769–772
 21. Castillo E, Lima JA, Bluemke DA (2003) Regional myocardial function: advances in MR imaging and analysis. *Radiographics* 23:127–140
 22. Finn JP, Nael K, Deshpande V et al (2006) Cardiac MR imaging: state of the technology. *Radiology* 241:338–354
 23. de Bazelaire CM, Duhamel GD, Rofsky NM et al (2004) MR imaging relaxation times of abdominal and pelvic tissues measured in vivo at 3.0T: preliminary results. *Radiology* 230:652–659
 24. Bookstein FL (1989) Principal warps: thin-plate splines and the decomposition of deformations. *IEEE Trans Pattern Anal Mach Intell* 6:567–585